

# A Subsynchronous Oscillation Suppression Method Based on Self-Adaptive Auto Disturbance Rejection Proportional Integral Control of Voltage Source Converter Based Multi-Terminal Direct Current System with Doubly-Fed Induction Generator-Based Wind Farm Access

Miaohong Su<sup>1</sup>, Haiying Dong<sup>1,2,\*</sup>, Kaiqi Liu<sup>1</sup> and Weiwei Zou<sup>1</sup>

<sup>1</sup>School of Automatic and Electrical Engineering, Lanzhou Jiaotong University, Lanzhou, 730070, China

<sup>2</sup>School of New Energy and Power Engineering, Lanzhou Jiaotong University, Lanzhou, 730070, China

\*Corresponding Author: Haiying Dong. Email: [hydong@mail.lzjtu.cn](mailto:hydong@mail.lzjtu.cn)

Received: 30 May 2020; Accepted: 28 July 2020

**Abstract:** A subsynchronous oscillation suppression strategy based on self-adaptive auto disturbance rejection proportional integral controller is proposed for doubly-fed induction generator-based wind farm integrated into grid through voltage source converter based multi-terminal direct current. In this strategy, the nonlinear PI controller is constructed by *fal* function to replace the traditional linear PI controller, and then the tracking differentiator is used to arrange the appropriate transition process in combination with the idea of active disturbance rejection control, and the self-adaptive auto disturbance rejection proportional integral controller is designed. By applying the controller to the inner loop of the converter on the rotor side of the doubly-fed induction generator, the adaptability of the control parameters of the inner loop to the change of operating conditions of the system can be improved, and the dynamic performance of the system can be improved. The simulation results on PSCAD/EMTDC show that, compared with SSDC, when the wind speed is 7.5 m/s, 8.5 m/s and 9.5 m/s, the convergence time can be shortened by 0.2 s, 0.1 s and 0.25 s, respectively. When the number of grid-connected doubly-fed induction generator wind turbines is 200 and 220, the convergence time is shortened by 0.1s. When the self-adaptive auto disturbance rejection proportional integral controller and the multi-channel variable-parameter additional subsynchronous damping controller work together, the convergence time under the above three wind speeds are 2.7 s, 2.7 s and 2.3 s, respectively. When the number of grid-connected doubly-fed induction generator wind turbines is 200 and 220, the convergence time is 2.65 s and 2.75 s, respectively. It can be concluded that the self-adaptive auto disturbance rejection proportional integral controller can realize the effective suppression of the subsynchronous oscillation under different operating conditions of the wind farm via the comparison with the additional subsynchronous damping control of doubly-fed induction generator. Besides, subsynchronous oscillation will converge faster and the stability of the system can be enhanced when the self-adaptive auto disturbance rejection proportional integral controller and the multi-channel variable-parameter additional subsynchronous damping controller work together.



This work is licensed under a Creative Commons Attribution 4.0 International License, which permits unrestricted use, distribution, and reproduction in any medium, provided the original work is properly cited.

**Keywords:** Doubly-fed induction generator; voltage source converter based multi-terminal direct current; subsynchronous oscillation; self-adaptive auto disturbance rejection proportional integral controller

## 1 Introduction

Voltage source converter based multi-terminal direct current (VSC-MTDC) has become the main transmission mode of large-scale new energy transmission due to its unique technical advantages. However, the stability control of the system is facing new challenges with the intergration of large-scale new energy. When wind power is sent out via VSC-MTDC system, the interaction mechanism between wind power controllers and VSC-MTDC controllers is intertwined, which makes the interaction mechanism between the two more complicated. There is the risk of subsynchronous oscillation (SSO), which has a certain influence on the safe and stable operation of the power grid. Therefore, the suppression of SSO needs to be solved urgently [1–3].

In order to solve above problems, scholars at home and abroad have done a lot of research on this problem. In [4], the SSO caused by offshore wind farms integrated into grid through VSC-HVDC system is studied based on the small signal model, and the suppression strategies based on subsynchronous damping control (SSDC) of doubly-fed induction generator (DFIG) side and VSC side are proposed, respectively. In [5], novel damping controllers are designed at the wind turbine side and the VSC-HVDC converter to suppress the power oscillation caused by the wind farm integrated into grid through VSC-HVDC. In [6], SSO caused by DFIG-based wind farm integrated into grid through modular multilevel converter based HVDC (MMC-HVDC) system is studied, and the suppression strategy based on the additional subsynchronous oscillation current suppression of the sending end converter is proposed. In [7], the methods of increasing the virtual resistance in MMC bridge arms, adopting the resonant voltage compensation and harmonic circulation suppression in the converter which connected with wind power plant are proposed for the SSO caused by DFIG-based wind farm integrated into grid through MMC-HVDC system. In [8], the coordinated optimization strategy of the multi-channel PSS and thyristor controlled series compensator (TCSC) damping controller is researched in order to suppress both the low-frequency oscillation and SSO. In [9], the SSO characteristics of direct driven wind farm interfaced with MMC-HVDC system is studied based on the impedance model, and the damping control strategy with series virtual resistance in MMC controller is proposed. In [10], in order to suppress the subsynchronous control interaction caused by the converter control and the series capacitance in the series compensation transmission system with DFIG-based wind farm integration, a novel suppression strategy of DFIG based on active disturbance rejection control (ADRC) is proposed. In [11], aiming at the SSO problem of the multi-feed hybrid flexible DC transmission system with DFIG-based wind farm access, the damping controllers of two DC transmission lines are designed respectively via the pole assignment method based on the modal control theory. However, changes of operating conditions of wind farms make the oscillation frequency time-varying. At present, there is little literature about SSO suppression strategy and its design method adapted to multiple operating conditions.

In view of the shortcomings of the above studies, this paper combines ADRC and nonlinear PI control, and introduced the *fal* function to realize the optimal setting of PI parameters [12]. Based on the above control idea to improve the control strategy of the DFIG rotor side converter (RSC) via self-adaptive auto disturbance rejection proportional integral (SAADR-PI) controller to replace the traditional PI control. Finally, the effectiveness of the suppression strategy is verified by time-domain simulation.

The main contributions of this paper are as follows: 1). The mechanism of SSO caused by DFIG-based wind farm integrated into grid through VSC-MTDC system is revealed. 2). The SAADR-PI controller is designed to suppression the SSO. 3). The effectiveness of SAADR-PI is verified, the conclusion that the

suppression effect of SAADR-PI and multi-channel variable-parameter SSDC when synergistic is better than that of the two when they work alone.

The remainder of the paper is organized as follows: In Section 2, the structure of the system is shown and the mechanism of SSO caused via DFIG-based wind farm integrated with VSC-MTDC system is described. Section 3 describes SSO suppression strategies of RSC and VSC-MTDC converter. Section 4 verifies the effectiveness of suppression strategies by time-domain simulation. Finally, conclusions are drawn in Section 5.

## 2 System Structure and Mechanism of SSO

### 2.1 Structure of the System

The structure of the system studied in this paper is shown in Fig. 1. The wind farm is composed of DFIGs, and the unit adopts the form of “one machine and one transformer.” The single wind turbine unit is fed into 35 kV collector line through the machine-end transformer. With a little local load near the wind farms and then connected to the VSC-MTDC system through 35/330/750 kV step-up transformer. This paper focuses on the study of SSO caused by the interaction between DFIG-based wind farm and VSC-MTDC system. The interaction between wind turbines is not considered. Therefore, the large-capacity wind farm is equivalent to a single DFIG.

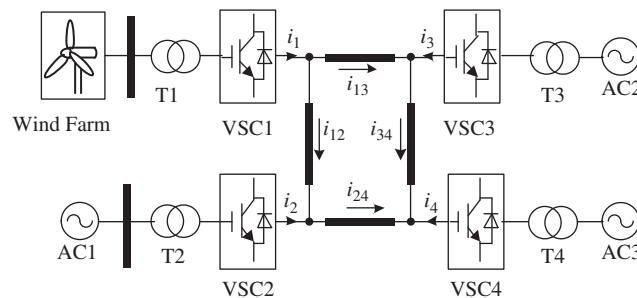


**Figure 1:** Structure of DFIG-based wind farm integrated into grid through VSC-MTDC system

VSC-MTDC converters mostly adopt the double closed-loop control of outer loop active power control and inner loop current control, and its control block diagram is shown in Fig. 2 [13]. When the system is in normal operating condition, VSC1 controls the amplitude of voltage and frequency at point of common

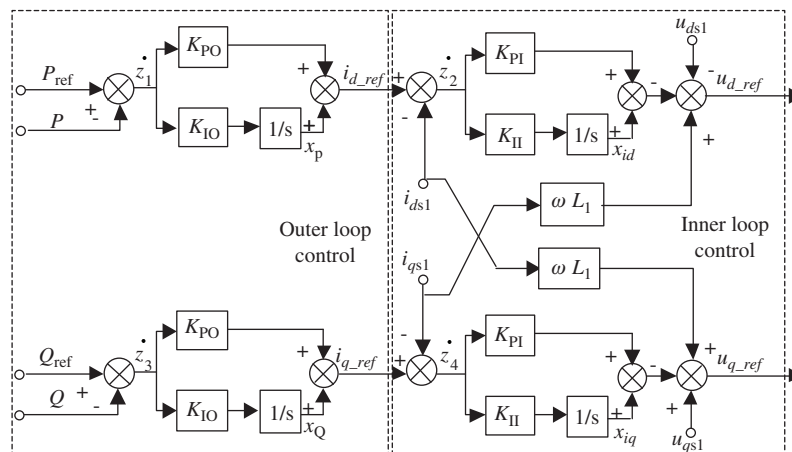


**Figure 2:** Active power and reactive power control block diagram

coupling (PCC) of the wind farm, and provides a stable AC power for the wind farm. As the main station, VSC3 controls the voltage stability of the DC bus and provides a certain amount of reactive power to the AC grid. Both VSC2 and VSC4 use active power control.

In Fig. 2,  $P_{ref}$  and  $P$  are the reference and measured values of the input active power;  $Q_{ref}$  and  $Q$  are the reference and measured values of the input reactive power;  $K_{PO}$  and  $K_{IO}$  are the proportionality and integral coefficients of the outer loop controller;  $K_{PI}$  and  $K_{II}$  are the proportionality and integral coefficients of the inner loop controller.

DFIG is composed of wind turbine, doubly-fed induction generator, RSC, grid side converter (GSC) and its control system, as well as filter circuit, etc. [14]. The shafting of DFIG adopts a two-mass shafting model, and converters of both sides adopt the double-closed loop control strategy. The RSC controls the active power of the generator and maintains the generator terminal voltage constant. The control objective of the GSC is to keep capacitance voltage constant and controls the output reactive power of the system. The control block diagram is shown in Fig. 3.

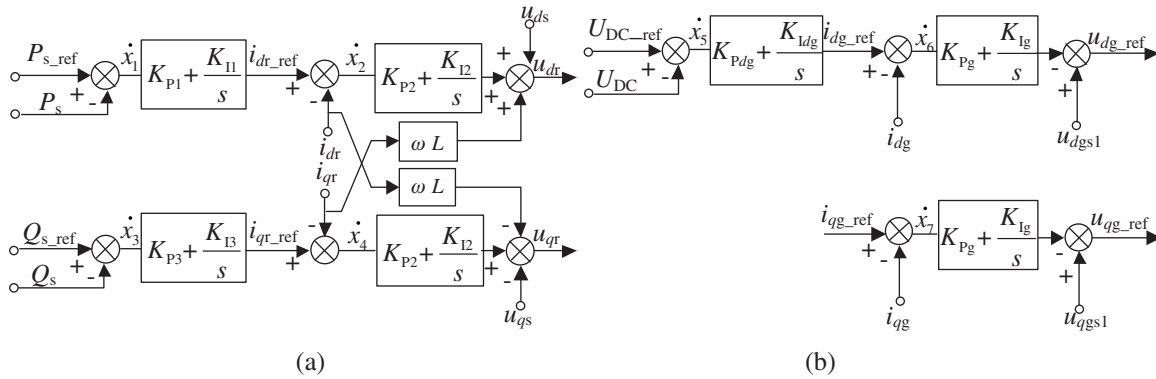


**Figure 3:** Control block diagram of DFIG, (a) RSC, (b) GSC

In Fig. 3, the  $d$ -axis controller of the outer loop of the rotor side ensures the stator active power tracking reference value,  $K_{p1}$  and  $K_{i1}$  are proportion and integral coefficients of which. The  $q$ -axis controller guarantees the stator reactive power tracking reference value,  $K_{p3}$  and  $K_{i3}$  are proportion and integral coefficients of the outer loop controller;  $K_{p2}$  and  $K_{i2}$  are proportion and integral coefficients of the inner loop controller. The  $d$ -axis controller of the outer loop of the grid side maintains the voltage stability of the DC bus of the converter,  $K_{pdg}$  and  $K_{idg}$  are proportion and integral coefficients of which. The  $q$ -axis controller controls the exchange of reactive power,  $K_{pg}$  and  $K_{ig}$  are the proportion and integral coefficients.

## 2.2 Generation Mechanism of SSO

When the DFIG-based wind farm integrated into grid through VSC-MTDC system, the SSO is mainly related to the interaction between DFIG controller and VSC-MTDC converter controller [15,16].

In Fig. 4,  $e_s$  and  $e_r$  are the induced electromotive force of the stator and the rotor;  $u_r$ ,  $u_g$ ,  $u_s$ ,  $u_c$  and  $E_{dc}$  are rotor voltage, grid side voltage, terminal voltage, VSC output converter voltage and equivalent DC source, respectively;  $L_c$  is the combined value of VSC-MTDC buffer inductance and AC line inductance. As can be seen from the Fig. 4, the stator current  $i_s$  of the DFIG is jointly determined by  $u_c$ ,  $u_g$ , and  $e_s$ , and the output characteristic of  $u_c$  is affected by VSC controller, so VSC affects the stator current, that is, VSC affects the dynamic characteristics of the electromagnetic torque of the DFIG. Therefore, the coupling between the VSC-MTDC system and DFIG is realized through the electromagnetic torque.

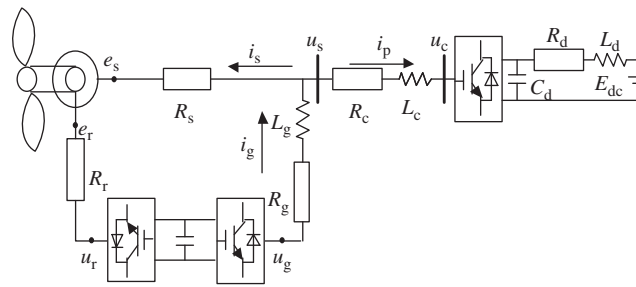


**Figure 4:** Schematic diagram of the mechanism of SSO

According to the analysis, when the torque increment  $\Delta T_e$  falls in the first and second quadrants of the torque-rotation complex plane, it is the negative damping characteristic, while it is the positive damping characteristic when it falls in the third and fourth quadrants [16]. However, the electromagnetic torque presents negative damping characteristics within a specific frequency range and SSO may occur when the parameters of VSC-MTDC controller and DFIG controller are not matched reasonably.

### 3 The SSO Suppression Measures of the System

Because it is a non-linear, multi-variable and strong coupling system, and the unreasonable match of controller parameters between VSC-MTDC and DFIG in subsynchronous conditions will cause the electromagnetic torque be negative damping characteristics. If a linear PI controller is adopted, the system voltage and current will be disturbed to some degree once a small disturbance occurs in the system. Therefore, from the perspective of control, this paper improves the stability of the system via improving the control strategy of RSC, so as to achieve the purpose of suppressing SSO.

#### 3.1 Suppression Principle of SSO

According to the complex torque coefficients method, the electrical damping coefficient and mechanical damping coefficient of the generator can be expressed as [17]:

$$\begin{cases} D_e = \text{Re}(\Delta T_e / \Delta \omega) \\ D_m = \text{Re}(\Delta T_m / \Delta \omega) \end{cases} \quad (1)$$

where  $\Delta T_e$  and  $\Delta T_m$  are the electromagnetic torque and mechanical torque increments of the generator,  $\Delta \omega$  is the angular velocity increment. The condition of  $D_e + D_m > 0$  must be satisfied when suppressing the SSO of the generator. Since  $D_m$  is always greater than 0, SSO can be suppressed only the phase difference between the  $\Delta \omega$  and  $\Delta T_e$  is between  $0^\circ$  and  $90^\circ$ .

The torque component is shown in Fig. 5.  $\Delta \delta$  is the power-angle increment of the generator,  $\Delta T_D$  and  $\Delta T_S$  are the damping torque component and the synchronous torque component.  $\Delta T_D$  is positive when the phase difference between  $\Delta \omega$  and  $\Delta T_e$  is between  $0^\circ$  and  $90^\circ$ .

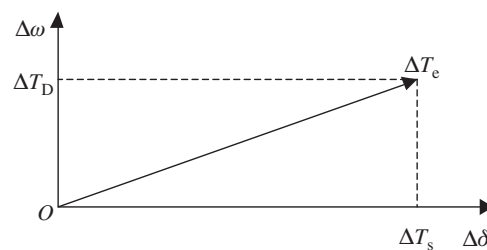


**Figure 5:** Torque component diagram

### 3.2 SSO Suppression Strategy of DFIG

#### 3.2.1 Design of SAADR-PI Controller

The classical PID controller adopts the linear combination of the error of the reference input and the controlled variable and its differential and integral to generate the control signal. Theoretical analysis and a lot of practice show that this linear control method with fixed parameters often leads to the contradiction between system rapidity and overshoot [18]. A large number of analytical studies show that the combination of these three state variables in some nonlinear form will help improve the effect of controller [18,19]. Therefore, this paper constructs a nonlinear PI controller by using nonlinear *fal* function.

*fal* function is a special nonlinear structure. The feedback link will generate a small feedback gain when the error signal of input is large, and a large feedback gain when the error signal is small by adjusting the parameters of *fal* function. It is a mathematical fitting of the control engineering experience of “small error, large gain” [18]. *fal* function has become a common nonlinear feedback structure because of fast convergence characteristics.

The *fal* function is expressed as follows:

$$fal(e, a, \delta) = \begin{cases} \frac{e}{\delta^{1-a}}, & |e| \leq \delta \\ |e|^a \text{sgn}(e), & |e| > \delta \end{cases} \quad (2)$$

where *a* is a constant between 0 and 1, which determines the nonlinearity of the nonlinear function *fal*;  $\delta$  is the constant that affects the filtering effect; *e* is the input error.

The combination form of nonlinear PI controller is as follows based on *fal* function [18]:

$$u = K_P fal(e, a_0, \delta_0) + K_I fal(e, a_1, \delta_1) \quad (3)$$

where  $K_P$  and  $K_I$  are proportion and integral coefficients of the PI segment. The composition of the nonlinear PI controller is shown in Fig. 6.

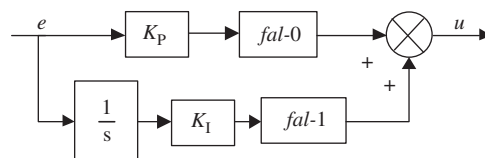


**Figure 6:** Structure of nonlinear PI controller

According to the design idea of nonlinear PI controller mentioned above, the SAADR-PI controller based on *fal* function is designed by taking the *d*-axis inner loop control of double closed-loop control as an example, and its structure is shown in Fig. 7 [12].

In Fig. 7,  $i_{d\_ref}$  is the reference value of *d*-axis current;  $i_d$  is the actual value of *d*-axis current;  $e_1$  is the error between the arranged transition process and the actual value of the *d*-axis current;  $u_d'$  is the output voltage value of the nonlinear PI link; tracking differentiator (TD) arranges the appropriate transition for the set value so that the variable can track the input signal “as fast as possible” within the limit of acceleration. TD in SAADR-PI controller is constructed by the nonlinear saturation function  $\text{sin}_{\text{sgn}}$ .

$$\begin{cases} \dot{x}_1 = x_2 \\ \dot{x}_2 = -\alpha \text{sin}_{\text{sgn}}(x_1 - i_{d\_ref} + \frac{x_2 |x_2|}{2\alpha}, \delta) \end{cases} \quad (4)$$

where

$$\sin_{\text{sgn}}(A, \delta) = \begin{cases} \text{sgn}(A), & |A| > \delta \\ \sin \frac{\pi A}{2\delta}, & |A| \leq \delta, \delta > 0 \end{cases} \quad (5)$$

$$\text{sgn}(A) = \begin{cases} 1, & A > 0 \\ 0, & A = 0 \\ -1, & A < 0 \end{cases} \quad (6)$$

where  $x_1$  is the tracking signal of  $i_{d\text{-ref}}$ ;  $x_2$  is the approximate derivative of  $i_{d\text{-ref}}$ ;  $\alpha$  is the accelerating factor.

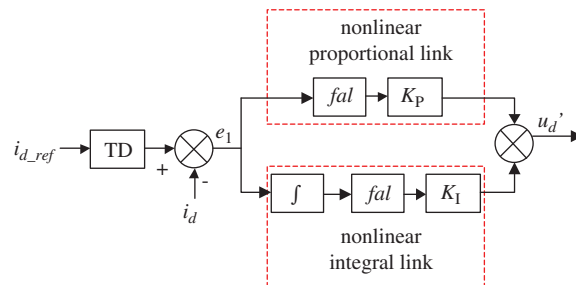


**Figure 7:** Structure diagram of SAADR-PI controller

### 3.2.2 Design of SSO Suppression Controller on RSC

It can be concluded that the inner loop proportional gain of the RSC has a great influence on SSO [15]. The existing control methods are mostly adding SSDC to the DFIG control strategy. SSDC can be attached to the outer loop with active power control. Its structure is shown in Fig. 8.

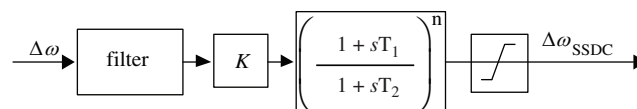


**Figure 8:** Structure block diagram of SSDC suppression strategy

Select the generator speed deviation as the input signal, the control signal of this oscillation frequency is generated through the band-pass filter and proportional phase shift link, thus generating additional subsynchronous electromagnetic torque, making the electrical damping of this oscillation frequency positive and suppressing SSO. SSDC has a good adaptability and suppression effect on the torsional vibration of shaft system with fixed oscillation frequency. However, the random fluctuation characteristic of wind power output leads to the uncertainty of oscillation frequency in actual operation. The SSDC suppression strategy designed for a specific oscillation frequency is not suitable for the SSO suppression problem where the oscillation frequency changes with time, which also brings new challenges to the suppression technology.

SAADR-PI controller has the advantages of fast response speed and strong anti-interference ability. Therefore, it can be applied to the inner loop of the RSC to replace the traditional PI controller to improve the adaptive ability and the stability of the system. The control block diagram of RSC based on SAADR-PI controller is shown in Fig. 9.

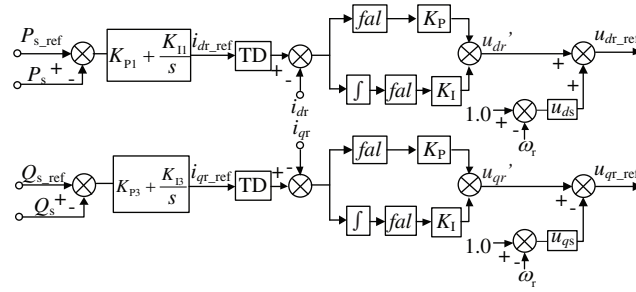


**Figure 9:** Control block diagram of RSC

In Fig. 9,  $P_{s\_ref}$  and  $P_s$  are the reference value and the measured value of active power input of the rotor side, respectively;  $Q_{s\_ref}$  and  $Q_s$  are the reference value and the measured value of corresponding reactive power, respectively;  $\omega_r$  represents rotor speed.

### 3.3 SSO Suppression Strategy of VSC-MTDC Converter

The SSO caused by wind power interfaced with VSC-MTDC is related to the interaction of control between the two. However, wind power, as a power source with randomness and volatility, cannot adapt to the change of operating conditions when using the traditional additional damping control, and the change of controller parameters will also have a certain impact on other modes of oscillation. Therefore, a multi-channel variable-parameter SSDC which is applicable to the system in the paper can be designed based on the design method of multi-channel variable-parameter [20], and its structure is shown in Fig. 10.

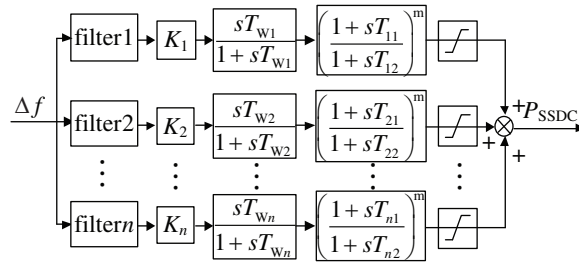


**Figure 10:** Schematic diagram of multi-channel SSDC structure

The structure embodies the design idea of modal separation, and separates the components through a band-pass filter to minimize the mutual influence between the phase compensation links. The design idea of variable-parameter enables the internal parameters to be adjusted with the change of operating conditions.

According to [20], the phase lag characteristic changes roughly linearly with the input power of the VSC-HVDC converter within the variation range of the input power. Since the angle of phase lag does not change dramatically with the input power of the VSC-HVDC converter, the phase compensation link lead/lag time constants  $T_1$  and  $T_2$  also change roughly linearly within the range of the input power [20]. In the system that studied in this paper, the input power of VSC-MTDC converter is equal to the output power of the wind farm when the transmission line loss is ignored. Therefore, the linear relationship between the output power of the wind farm and  $T_1$  and  $T_2$  can be obtained. Based on this, the multi-channel variable-parameter SSDC is designed, and its internal parameters can be adjusted in real time with the change of the output power of the wind farm, so as to achieve the purpose of optimal compensation angle.

### 4 Simulation

The following simulation is performed based on the system structure described in Section 2. The capacity of the wind farm is set to be 500 MW, the system operates at a subsynchronous condition with wind speed of 8.5 m/s and rotation speed of 0.8 pu. Some parameters of the system are shown in Tab. 1.

**Table 1:** System parameters

Parameters	Values	Parameters	Values
Output voltage of DFIG (kV)	0.69	Rated DC voltage of VSC1/kV	800
Rated wind speed (m/s)	12	Rated capacity of VSC1 (MW)	500
Rated rotor speed (pu)	1.2	Proportional/integral gain of VSC1 outer loop	0.8/10
Rated frequency (Hz)	50	Proportional/integral gain of VSC1 inner loop	0.5/10

#### 4.1 Comparison of Suppression Effect between SAADR-PI and SSDC

SSDC and the control strategy based on SAADR-PI controller are respectively adopted on the RSC, and the structure of SSDC is shown in Fig. 8. The suppression effect of two suppression methods on SSO under different operating conditions is analyzed. Assume that there is the sudden change of the load at  $t = 2$  s.

##### 4.1.1 Changes of the Wind Speed

Only change the wind speed and keep other operating conditions unchanged, the response characteristics of the output power of the wind farm with two suppression strategies are shown in Fig. 11.

As can be seen from Fig. 11, if no suppression measures are taken at the three wind speeds, the output power of the wind farm will be critical oscillation when the wind speed is 8.5 m/s; it will gradually diverge when the wind speed is 7.5 m/s and gradually converge when the wind speed is 9.5 m/s. However, SSO can be suppressed when SSDC and SAADR-PI are adopted, respectively. Fig. 11a shows that the convergence time of SSDC and SAADR-PI are 3.2 s and 3.0 s, respectively. Fig. 11b shows that the convergence time of

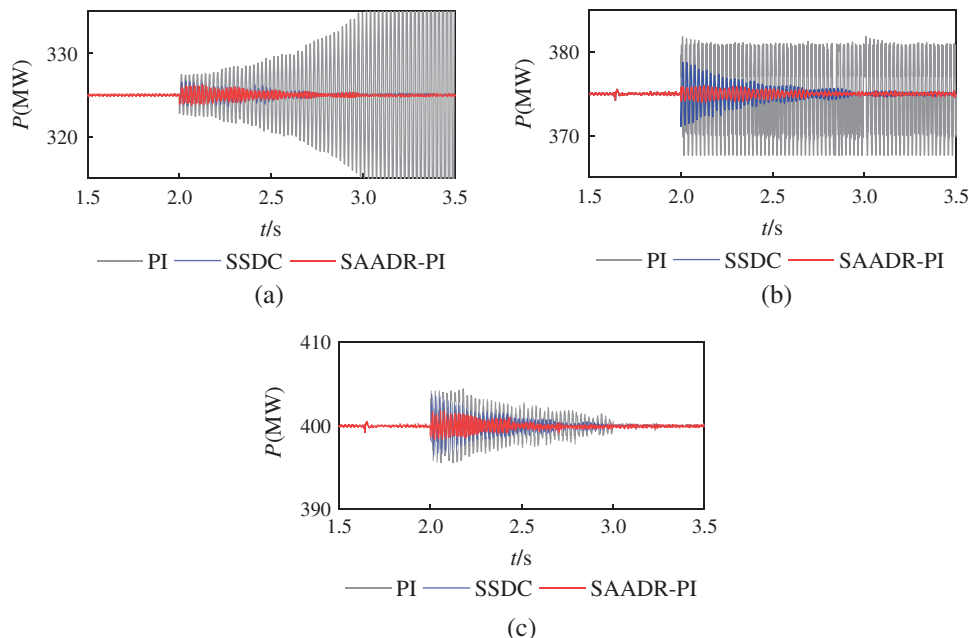


**Figure 11:** Output power of wind farm at different wind speeds, (a) 7.5 m/s, (b) 8.5 m/s, (c) 9.5 m/s

SSDC and SAADR-PI are 2.9 s and 2.8 s, respectively. Fig. 11c shows that the convergence time of SSDC and SAADR-PI are 2.7 s and 2.45 s, respectively. It can be concluded that SSO has a faster convergence rate and a smaller amplitude of oscillation when SAADR-PI control is adopted. Therefore, the SSO suppression effect is better when SAADR-PI controller is adopted.

#### 4.1.2 Changes in the Number of DFIGs Connected to the Grid

Set wind speed is 7.5 m/s, and keep other operating conditions unchanged. The output power response characteristics of wind farm is shown in Fig. 12 when the number of grid-connected DFIGs changes.

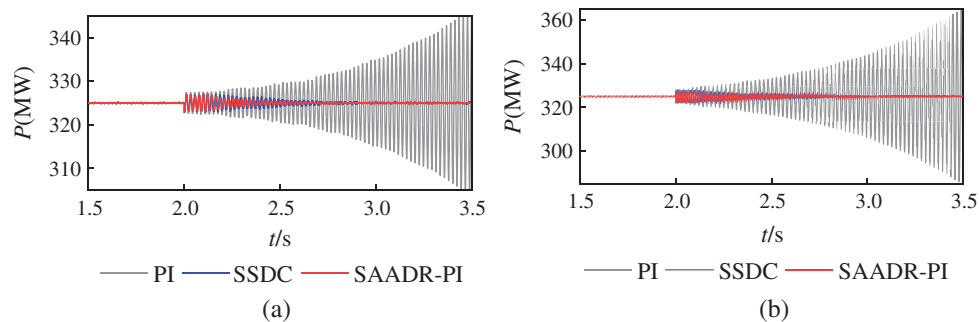


**Figure 12:** Wind farm output power when the number of grid-connected DFIGs changes, (a) 200, (b) 220

It can be seen from Figs. 11a and 12 that when there is no suppression measures are taken, the corresponding relationship between the system oscillation trend and wind speed remains unchanged as the increase of wind turbines put into operation, but the stability of the system deteriorates. In the first case, the output power will converge at 2.9 s when SSDC is adopted, while it will converge at 2.8 s when SAADR-PI is used. Similarly, in the second case, the output power will converge at 3.2 s when SSDC is adopted, while it will converge at 2.6 s when SAADR-PI is used. Therefore, the SSO can be suppressed to a certain extent when SSDC and SAADR-PI control-based suppression methods are used, respectively. However, the convergence rate of SSO is faster and the oscillation amplitude is smaller when SAADR-PI controller is adopted. Therefore, the suppression effect of SAADR-PI controller is better.

The above simulation results show that when the suppression measures are adopted only on DFIG, both suppression methods can have a certain suppression effect on SSO. However, compared with SSDC, the suppression strategy based on SAADR-PI controller on SSO is less affected by the operating conditions of the system, and has stronger adaptability to the fluctuation of wind power generation, thus the stability of the system is enhanced.

## 4.2 Simulation of SSO Based on VSC-SSDC Control

### 4.2.1 Changes of the Wind Speed

Keep the number of grid-connected DFIGs unchanged. No suppression measures are adopted on the DFIG side. Only multi-channel variable-parameter SSDC is used in the VSC-MTDC converter (VSC-SSDC). Fig. 13 shows the output active power responses of the wind farm to the sudden change of the load at  $t = 2$  s under different wind speeds.

From Figs. 13a–13c, it can be seen that the convergence time of VCSS-SSDC is 3.4 s, 3.25 s and 3.2 s, respectively. It can be concluded that multi-channel variable-parameter SSDC can also make the output power of wind farm at different wind speeds converges until stable within a certain time.

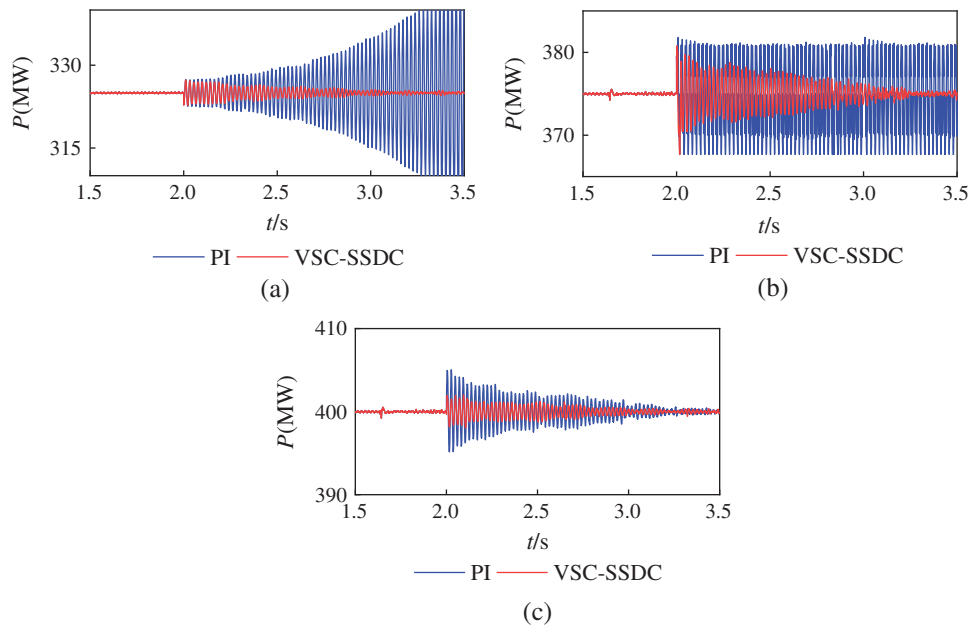


**Figure 13:** Output power of wind farm at different wind speeds, (a) 7.5 m/s, (b) 8.5 m/s, (c) 9.5 m/s

#### 4.2.2 Changes in the Number of DFIGs Connected to the Grid

Keep the wind speed at 7.5 m/s, only VSC-SSDC is used in the VSC-MTDC converter, and no suppression measures are taken on the DFIG side. Fig. 14 shows the output active power responses of the wind farm to the sudden change of the load at  $t = 2$  s when the number of grid-connected DFIGs changes.

Fig. 14a shows that the output power will converge at 3 s, and Fig. 14b shows that the output power will converge at 3.25 s. As can be seen from Fig. 14, when the number of DFIGs put into operation changes, VSC-SSDC can make the oscillation amplitude and frequency of SSO gradually decrease until stable.

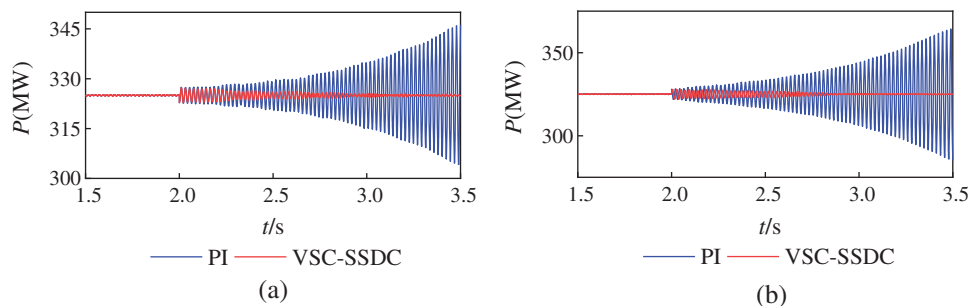


**Figure 14:** Wind farm output power when the number of grid-connected DFIGs changes, (a) 200, (b) 220

#### 4.3 Cooperative Suppression of SAADR-PI and VSC-SSDC

According to the above analysis, the control method of RSC based on SAADR-PI controller and the multi-channel SSDC on the VSC-MTDC converter have a certain suppression effect on SSO. Therefore, the suppression effect is analyzed in this section when the two suppression methods act simultaneously under different operating conditions. Similarly, assume that there is the sudden change of the load at  $t = 2$  s.

### 4.3.1 Changes of the Wind Speed

The simulation conditions are as shown in Section 4. The output power curves of the wind farm is shown in Fig. 15 when different suppression methods are adopted at different wind speeds.

From Figs. 15a and 15b, the output power will converge at 2.7 s when SAADR-PI and VSC-SSDC work simultaneously. In Fig. 15c, the output power will converge at 2.3 s when SAADR-PI and VSC-SSDC work simultaneously. From the above analysis, it can be concluded that when SAADR-PI controller and VSC-SSDC are adopted at the same time, the output power of the wind farm has the fastest convergence rate and the stability of the system is better.

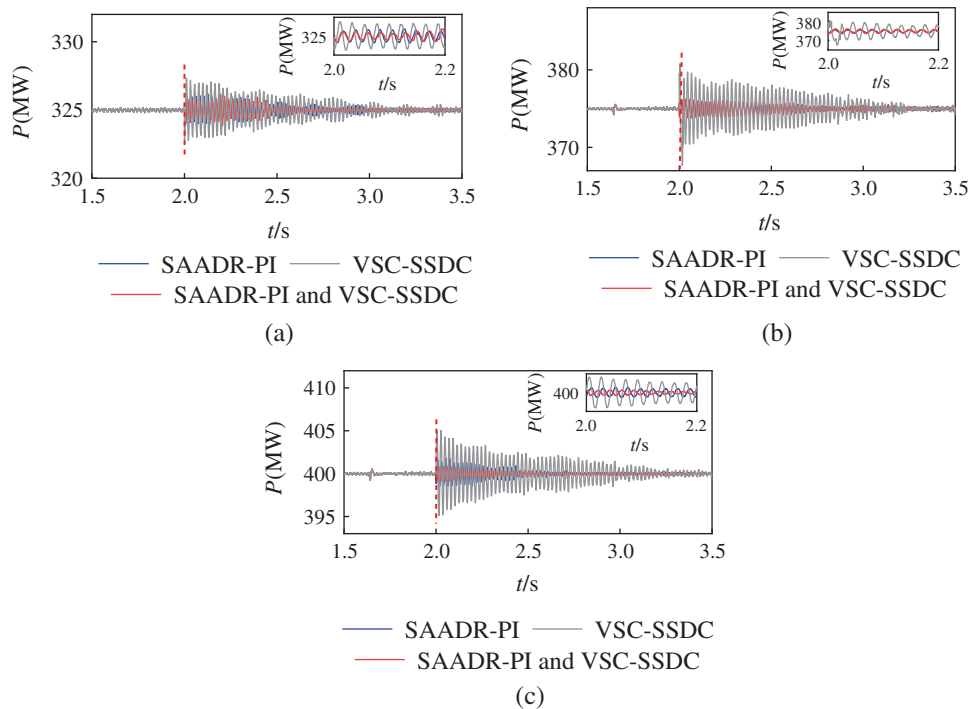


**Figure 15:** Comparison of output power when wind speed changes, (a) 7.5 m/s, (b) 8.5 m/s, (c) 9.5 m/s

### 4.3.2 Changes in the Number of DFIGs Connected to the Grid

The simulation conditions are as shown in Section 4. Fig. 16 shows the output power curves of wind farm when the number of DFIGs in operation is changed and different suppression strategies are adopted.

Fig. 16a shows that the output power will converge at 2.65 s when SAADR-PI and VSC-SSDC work simultaneously, and Fig. 16b shows that the output power will converge at 2.75 s when SAADR-PI and

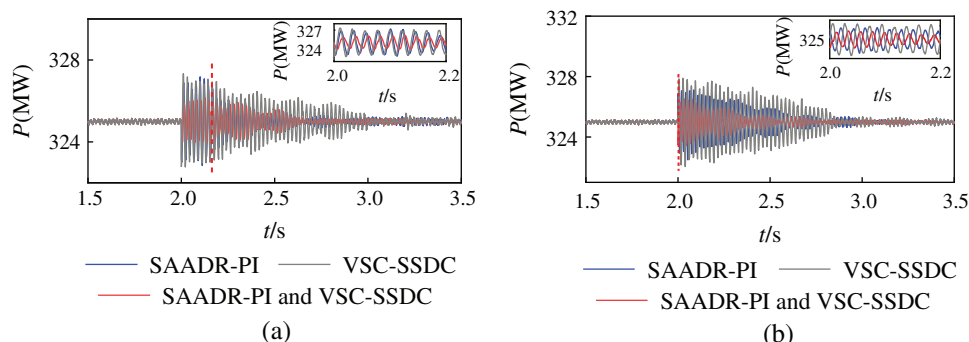


**Figure 16:** Comparison of output power when the number of grid-connected DFIGs changes, (a) 200, (b) 220

VSC-SSDC work simultaneously. As can be seen from Fig. 16, when the number of DFIGs in operation changes, compared with the single addition of SAADR-PI controller or VSC-SSDC, the output power of the wind farm can reach stability in the shortest time, and the risk of SSO in the system is reduced when SAADR-PI controller and VSC-SSDC are added together.

## 5 Conclusions

In order to solve the problem of SSO caused by DFIG-based wind farm integrated into grid through VSC-MTDC system, the suppression strategy of DFIG rotor-side controller based on SAADR-PI controller is designed. The following conclusions can be obtained:

(1) By using SSDC and SAADR-PI controllers on the RSC respectively to analyze the suppression effect of SSO, the control strategy of RSC based on SAADR-PI controller combines the advantages of ADRC and traditional PI control, which can realize the stable and fast dynamic regulation of the system. Compared with SSDC, this control strategy can suppress SSO more effectively.

(2) When the wind speed or the number of grid-connected DFIGs changes, the SSO of the system can be effectively suppressed.

(3) When the suppression measures are adopted on the DFIG and VSC-MTDC converter at the same time, the SSO of the system decays rapidly and the suppression effect is better. The stability of the system is improved significantly.

**Funding Statement:** This work was supported by the Key Research and Development Project of Gansu Province (18YF1GA056).

**Conflicts of Interest:** The authors declare that they have no conflicts of interest to report regarding the present study.

## References

1. Chen, C., Du, W. J., Wang, H. F. (2018). Review on mechanism of sub-synchronous oscillations caused by grid-connected wind farms in power systems. *Southern Power System Technology*, 12(1), 84–93.
2. Amin, M., Molinas, M. (2017). Understanding the origin of oscillatory phenomena observed between wind farms and HVdc systems. *IEEE Journal of Emerging and Selected Topics in Power Electronics*, 5(1), 378–392. DOI 10.1109/JESTPE.2016.2620378.
3. Xie, X. R., Liu, H. K., He, J. B., Liu, H., Liu, W. (2018). On new oscillation issues of power system. *Proceedings of the CSEE*, 38(10), 2821–2828+3133.
4. Bian, X. Y., Ding, Y., Mai, K., Zhou, Q. B., Zhao, Y. et al. (2018). Sub-Synchronous oscillation caused by grid-connection of offshore wind farm through VSC-HVDC and its mitigation. *Automation of Electric Power Systems*, 42(17), 25–39.
5. Zeni, L., Eriksson, R., Goumalatsos, S., Altin, M., Sorensen, P. et al. (2016). Power oscillation damping from VSC-HVDC connected offshore wind power plants. *IEEE Transactions on Power Delivery*, 31(2), 829–838. DOI 10.1109/TPWRD.2015.2427878.
6. Lyu, J., Cai, X., Amin, M., Molinas, M. (2018). Sub-synchronous oscillation mechanism and its suppression in MMC-based HVDC connected wind farms. *IET Generation, Transmission & Distribution*, 12(4), 1021–1029. DOI 10.1049/iet-gtd.2017.1066.
7. Lyu, J., Molinas, M., Cai, X. (2017). Stabilization control methods for enhancing the stability of wind farm integration via an MMC-Based HVDC System. *11th IEEE International Conference on Compatibility, Power Electronics and Power Engineering*, 324–329.
8. Chen, B. P., Lin, T., Chen, R. S., Zhang, J. N., Xu, X. L. (2016). *Coordinative optimization of multi-channel PSS and TCSC damping controller to suppress the low-frequency and subsynchronous oscillation*. Boston, MA: IEEE Power and Energy Society General Meeting, 1–5.

9. Guo, X. S., Li, Y. F., Xie, X. T., Hou, Y. L., Zhang, D. (2020). Sub-synchronous oscillation characteristics caused by PMSG-based wind plant farm integrated via flexible HVDC system. *Proceedings of the CSEE*, 40(4), 1149–1160,1407.
10. Gao, B. F., Hu, Y. T., Li, R., Yao, L., Zhao, S. Q. (2019). Research on subsynchronous control interaction mitigation strategy based on active disturbance rejection control for doubly-fed induction generator. *Power System Technology*, 43(2), 691–700.
11. Wang, L., Yang, Z. H., Lu, X. Y., Prokhorov, A. V. (2017). Stability analysis of a hybrid multi-infeed HVDC system connected between two offshore wind farms and two power grids. *IEEE Transactions on Industry Applications*, 53(3), 1824–1833. DOI 10.1109/TIA.2017.2672669.
12. Xu, J. Z., Cheng, H. J., Huang, W., Liu, Y. X., Chen, Z. Y. et al. (2018). A novel approach based on self-adaptive auto disturbance rejection proportional integral controller to suppress low frequency oscillation of high speed railway electric multiple units-traction network coupling system. *Proceedings of the CSEE*, 38(14), 4035–4045.
13. Lu, X. J., Lin, W. X., Wen, J. Y., Li, Y. F., Wu, Y. L. et al. (2016). Modularized small signal modelling method for DC grid. *Proceedings of the CSEE*, 36(11), 2880–2889.
14. Xie, D., Feng, J. Q., Lou, Y. Ch, Yang, M. X., Wang, X. T. (2013). Small-signal modeling and modal analysis of DFIG-based wind turbine based on three-mass shaft model. *Proceedings of the CSEE*, 33(S1), 21–29.
15. Sun, K., Yao, W., Wen, J. Y. (2018). Mechanism and characteristics analysis of subsynchronous oscillation caused by DFIG-based wind farm integrated into grid through VSC-HVDC system. *Proceedings of the CSEE*, 38(22), 6520–6533.
16. Song, S. H., Zhao, S. Q. (2020). Analysis of sub-synchronous oscillation of DFIG-based wind farm integrated to grid through VSC-HVDC system based on torque method. *Power System Technology*, 44(2), 630–636.
17. Gao, B. F., Yao, L. (2018). Supplementary damping control of SSO based on fuzzy active disturbance rejection control for photovoltaic-thermal-bundled system transmitted by series compensation. *Electric Power Automation Equipment*, 38(7), 121–127.
18. Li, H., Shang, J. N., Chen, Y., Shang, Q., Hao, R. X. et al. (2014). The applications of nonlinear PI controller based on the *fal* function in the DC-DC converter. *Transactions of China Electrotechnical Society*, 29(S1), 326–331.
19. Han, J. Q. (2017). Auto disturbances rejection control technique. *Frontier Science*, 1(1), 24–31.
20. Jiang, P., Hu, T., Wu, X. (2011). Multi-channel supplementary damping control in VSC-HVDC for SSO suppression. *Electric Power Automation Equipment*, 31(9), 27–31.